Non-anomalous magnetization density distribution in CeB_6

2003 J. Phys.: Condens. Matter 15 3095

(http://iopscience.iop.org/0953-8984/15/19/311)

INSTITUTE OF PHYSICS PUBLISHING JOURNAL OF PHYSICS: CONDENSED MATTER

J. Phys.: Condens. Matter **15** (2003) 3095–3106 PII: S0953-8984(03)58815-4

Non-anomalous magnetization density distribution in CeB_6

F Givord[1,4,5], J-X Boucherle[1,5], P Burlet[1,5], B Gillon[2,5] and S Kunii[3]

[1] CEA/DSM, Département de Recherche Fondamentale sur la Matière Condensée, SPSMS/MDN, 38054 Grenoble Cedex 9, France
[2] Laboratoire Léon Brillouin, CEA/Saclay, 91191, Gif sur Yvette, France
[3] Department of Physics, Tohoku University, Sendai, Miyagi 980-8578, Japan

E-mail: givord@drfmc.ceng.cea.fr

Received 27 January 2003, in final form 4 April 2003
Published 6 May 2003
Online at stacks.iop.org/JPhysCM/15/3095

Abstract

Results of polarized neutron diffraction on the compound CeB_6 are used to obtain its magnetization density distribution. The measurements are performed at two different points of the magnetic phase diagram (phase I and II). The data are analysed in direct space using the maximum entropy method, as well as in reciprocal space using the cerium form factor expansion and anisotropy. The conclusion is that, in both phases, the magnetization is localized on the cerium sites only. This result is in contradiction to a recent paper by Saitoh *et al* (2002 *J. Phys. Soc. Japan* **71** 2369), claiming that, in phase II, a localized spin moment was observed at non-atomic sites.

1. Introduction

For more than 20 years, the dense Kondo compound CeB_6 has been the subject of numerous experimental and theoretical studies. This compound with a simple cubic crystal structure (CsCl type) presents quite peculiar magnetic properties [1, 2], with phase transitions when an external magnetic field is applied. The field–temperature diagram [3] (figure 1) shows three main phases: a high temperature paramagnetic phase (phase I), an intermediate phase (phase II) which is believed to reflect antiferro-quadrupolar ordering and a complex antiferromagnetic phase (phase III) below $T = 2.3$ K in zero field. The mechanism of the magnetic ordering in phase II is not yet elucidated although it has been investigated a lot by experimental techniques such as neutron diffraction [4, 5], NMR [6], as well as by theoretical studies [7, 8].

The polarized neutron diffraction technique leads, with an excellent accuracy, to the magnetic structure factors $F_M(hkl)$ for a magnetic structure aligned along the applied field (ferromagnet or saturated paramagnet). These structure factors are the Fourier components of

[4] Author to whom any correspondence should be addressed.
[5] CNRS staff.

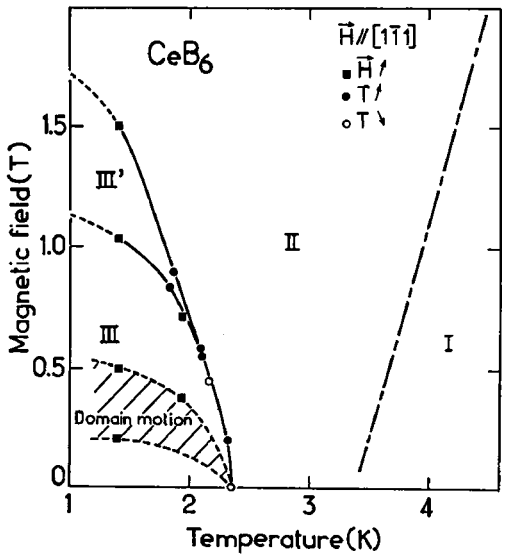

Figure 1. Magnetic phase diagram of CeB_6, from [3].

the magnetization density. By a Fourier summation it is, in principle, possible to obtain the magnetization density for each point of the unit cell

$$m(\boldsymbol{r}) = \sum_{Q} F_M(\boldsymbol{Q}) \exp(-\mathrm{i}\boldsymbol{Q} \cdot \boldsymbol{r}).$$

But, due to experimental limitations, only the projection on a plane perpendicular to the applied field can in general be obtained. Moreover the limited set of measured F_M induces some systematic errors in the observed map. It is only by use of the fairly recent and powerful method based on the maximum entropy that more accurate maps can be obtained and that a precise analysis can be made in direct space [9]. It is then possible to separate diffuse and localized densities. The measurement of the $F_M(hkl)$ also leads to the analysis, in reciprocal space, of the 4f contribution, in terms of the magnetic form factor. Its extension and anisotropy (dispersion around an average curve) are characteristic of the ground state wavefunction of the 4f ion. It is then possible to get information about the state of the ion and adjust crystal field and exchange parameters. Among the rare earths, the Ce^{3+} ion is specially convenient for such an analysis [10].

In 1981, polarized neutron diffraction measurements had been performed in phase II (at $T = 4.2$ K for a magnetic field H of 4 T applied along the twofold and fourfold cubic axes) [11]. The cerium magnetic form factors thus obtained for the two directions revealed that it could not correspond to a Γ_7 doublet as expected for Kondo systems, but to a Γ_8 quartet. It is now well established that the CeB_6 ground state is of Γ_8 type [12–14]. The magnetization density maps obtained by Fourier transformation were not published because they did not bring any relevant information to the problems raised at that time. New polarized neutron diffraction data have been recently published [15] and the authors find, by using the maximum entropy method, a spin density distribution with 'significant amounts of localized spin moment at non atomic sites'. A muon spin rotation experiment [16] leads to the same conclusion.

We have analysed the polarized neutron data of 1981 using the maximum entropy method and the form factor analysis, in order to check the magnetization distribution. Data which had been measured later in the paramagnetic state (phase I), and had not been published, are also presented.

Table 1. Parameters of the crystal structure of CeB_6. b is the Fermi length; B_{RT} and B_{LT} are the isotropic Debye–Waller factors obtained at room temperature and estimated at low temperature, respectively. The refined extinction factor g is 1900(120) rad^{-1}.

Space group: $Pm\bar{3}m$, $a = 4.025$ Å						
Site	x	y	z	b (fm)	B_{RT} (Å^2)	B_{LT} (Å^2)
Ce(1a)	1/2	1/2	1/2	4.84(5)	0.55(3)	0.15(5)
B(6e)	0.3004(2)	0	0	6.50(15)	0.36(2)	0.10(5)

Table 2. Experimental conditions for the various polarized neutron experiments.

Exp. no	Reactor	T (K)	H (T)	Axes	Phase	λ (Å)	Number of non-equivalent reflections
1	LLB	10	5	$[1\bar{1}0]$	I	0.73	32
2	ORNL	4.2	4	$[1\bar{1}0]$	II	0.78	38
3	ORNL	4.2	4	[100]	II	0.78	24

2. Measurements

The single crystals of CeB_6 were grown by the floating zone method, using 99% enriched ^{11}B to avoid the large neutron absorption due to ^{10}B. A crystallographic study was performed on a small sample of 0.7 mm^3 at room temperature [11]. All the parameters of the structure are gathered in table 1. This determination demonstrated that the extinction effects are far from negligible. The sample used for polarized neutron diffraction was a parallelepiped of $1 \times 1.8 \times 6$ mm^3. The largest dimension is a $[1\bar{1}0]$ cubic direction and the intermediate is the [001] one. The former measurements of the flipping ratios R were performed at the high flux isotope reactor of the ORNL (Oak Ridge, USA) and the latter ones at the LLB (Saclay, France). Short wavelengths were chosen in order to minimize the extinction effects and to allow collection of data up to $\sin\theta/\lambda = 0.9$ Å^{-1}. The conditions of each experiment (denoted 1, 2 and 3) are given in table 2.

Knowing the values of the flipping ratios $R = I^+/I^- = (1+\gamma)^2/(1-\gamma)^2$ of a Bragg reflection (hkl) yields the value of $F_M(hkl)$ through $\gamma = F_M/F_N$, where F_N and F_M are the nuclear and magnetic structure factors, respectively. For a correct determination of F_M, it is necessary to have, first, a good determination of γ, by making the appropriate corrections due to the device (polarization of the incident beam, flipping efficiency, $\lambda/2$ corrections) and secondly a good knowledge of the nuclear structure factors F_N and of the extinction effects in the sample. It is also important to detect possible sources of errors in the measurements of R, in relation to peculiar values of some structure factors.

3. Results and discussion

The $F_M(hkl)$ are the Fourier components of the magnetization density $m(\boldsymbol{r})$. Their values, together with the corresponding F_N values, are given in tables 3, 4 and 5, for the three experiments respectively. The $F_M(000)$ value is the magnetization measured in the same experimental conditions. The corresponding cerium magnetic amplitudes $\mu f(\boldsymbol{Q})$ (μ is the 4f magnetic moment and $f(\boldsymbol{Q})$ the magnetic form factor for the scattering vector $\boldsymbol{Q}$, with $|\boldsymbol{Q}| = 4\pi \sin\theta/\lambda$) is directly obtained from $F_M(\boldsymbol{Q})$. As the $\boldsymbol{Q}$ dependence of the cerium form factor is correlated to the ground state wavefunction [10], the form factor depends on the

Table 3. Nuclear structure factors F_N and magnetic structure factors without extinction correction F_{M0} and with extinction correction F_M, for experiment 1 at LLB.

(hkl)	$\sin(\theta)/\lambda$ (Å^{-1})	F_N (10 fm/CeB_6)	F_{M0} $g = 0$ (μ_B/CeB_6)	F_M $g = 1000(300)$ (μ_B/CeB_6)
(000)	0.0		0.250(10)	
(001)	0.123	1.709	−0.198(6)	−0.228(11)
(110)	0.174	0.971	0.220(4)	0.233(5)
(111)	0.213	−1.690	−0.191(4)	−0.211(7)
(002)	0.246	2.022	0.165(4)	0.183(7)
(112)	0.301	−1.363	0.176(6)	0.183(7)
(220)	0.348	−0.311	0.141(12)	0.141(12)
(221)	0.369	−2.941	−0.135(6)	−0.164(9)
(003)	0.369	3.134	−0.121(6)	−0.142(8)
(113)	0.408	−0.228	−0.110(18)	−0.111(18)
(222)	0.426	−2.616	0.123(5)	0.139(7)
(004)	0.492	3.385	0.083(5)	0.096(6)
(223)	0.507	−1.478	−0.118(5)	−0.122(5)
(114)	0.522	0.056	0.014(9)	0.014(9)
(330)	0.522	3.788	0.087(6)	0.109(8)
(331)	0.536	1.198	−0.134(12)	−0.137(12)
(332)	0.577	1.492	0.104(5)	0.108(6)
(224)	0.603	−1.187	0.087(5)	0.089(6)
(005)	0.615	0.794	−0.089(7)	−0.090(7)
(115)	0.639	−2.480	−0.067(4)	−0.072(4)
(333)	0.639	2.590	−0.086(9)	−0.094(9)
(440)	0.696	2.430	0.079(5)	0.085(5)
(225)	0.707	−3.679	−0.047(5)	−0.055(5)
(334)	0.717	2.827	0.064(5)	0.070(5)
(006)	0.738	3.306	0.054(8)	0.060(8)
(443)	0.788	1.285	−0.054(8)	−0.055(8)
(444)	0.852	1.520	0.045(13)	0.047(13)
(007)	0.861	2.945	−0.046(6)	−0.050(6)
(550)	0.870	−0.773	0.050(9)	0.050(9)
(551)	0.878	−3.213	−0.050(6)	−0.055(6)
(336)	0.904	2.764	0.020(6)	0.022(6)
(552)	0.904	−2.933	0.034(7)	0.037(7)
(227)	0.929	−1.395	−0.043(8)	−0.044(8)

value and direction of the applied field. We have therefore drawn in figure 2 three form factors corresponding to the three different experiments 1, 2 and 3. For each experiment, we have reported the values obtained without taking into account the extinction corrections ($g = 0$) and those obtained with an extinction parameter $g = 1000(300)$ rad^{-1} (corresponding to a mosaicity $\eta = (2\sqrt{\pi}g)^{-1} = 1'$). This value is not that refined from the crystallographic study because this experiment was performed on another crystal. It has been chosen to fit together the three polarized neutron experiments, which had been performed on one and the same crystal, by comparing strong reflections very sensitive to g and medium ones lying at close values of $\sin\theta/\lambda$. The corrected points show much less deviation from the common shape expected for a form factor dependence with $\boldsymbol{Q}$. However, one can notice that a few reflections, the (114) one in figure 2(1) and the (114), (441) and (116) ones in figure 2(2), are totally outside the form factor variation. For these three reflections, the value of F_N is extremely weak, one order

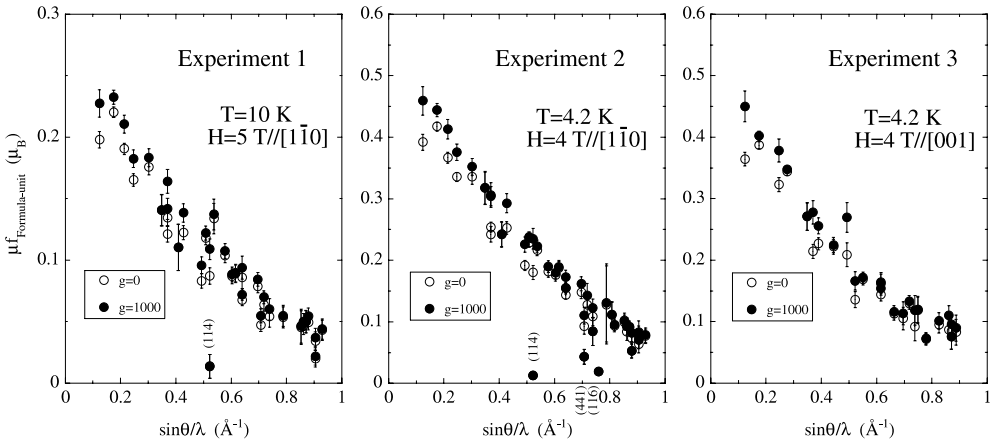

Figure 2. Magnetic amplitudes $\mu f(\boldsymbol{Q})$ for three experiments, without and with extinction corrections.

of magnitude less than the next weak reflection (see tables 3 and 4). Consequently, extinction does not play any role in these reflections but the measurement of the flipping ratio can be very easily falsified by any pertubation (multiple diffraction, imprecise $\lambda/2$ contamination, ...). The calculated error bars on these reflections are very small because of the almost zero value of F_N, and do not take into account these external sources of errors.

As the $F_M(hkl)$ were collected in the equatorial plane perpendicular to the applied field direction, the projection of the density onto that plane was calculated using the 2D maximum entropy method (MaxEnt) [17]. In the classical Fourier synthesis, the value of the Fourier components is taken as zero for all unmeasured reflections. The main advantage of the MaxEnt technique is that it makes no assumption concerning unmeasured Fourier components. It also takes into account experimental uncertainties. The number of pixels chosen for the MaxEnt calculations were 90×64 for projections on planes $(1\bar{1}0)$ and 64×64 for projections on planes (001), in order to always have pixels of the same size. The projected maps thus obtained for the three experiments are drawn in figures 3, 4 and 5. Figures 3(a), 4(a) and 5(a) are obtained by using all the measured reflections and without any extinction corrections. In fact, figures 3(a) and 4(a), corresponding to projections along a $[1\bar{1}0]$ direction, show some non-negligible positive contours outside the cerium sites. As the measurements on very weak reflections (114), (441) and (116) are probably fallacious, it is better to use MaxEnt without these reflections than with wrong values that might strongly affect the resulting maps. The maps shown in figures 3(b) and 4(b) were obtained without these spurious reflections and the magnetic density outside the cerium sites has disappeared. Figures 3(c), 4(c) and 5(b) correspond to data corrected for extinction. These maps look quite similar to the preceeding ones, showing that extinction corrections, which strongly affect the magnetic amplitudes in the form factor variation, are not of primary importance for the MaxEnt maps. Finally, magnetic contours are observed only on the cerium sites.

4. Form factor analysis

Knowing the $4f^1$ wavefunctions

$$|\psi\rangle = \sum_M a_M |J, M\rangle$$

Table 4. Nuclear structure factors F_N and magnetic structure factors without extinction correction F_{M0} and with extinction correction F_M, for experiment 2 at ORNL with the field applied parallel to $[1\bar{1}0]$.

(hkl)	$\sin(\theta)/\lambda$ (Å^{-1})	F_N (10 fm/CeB_6)	F_{M0} $g = 0$ (μ_B/CeB_6)	F_M $g = 1000(300)$ (μ_B/CeB_6)
(000)	0.0		0.480(10)	
(001)	0.123	1.709	−0.392(13)	−0.459(23)
(110)	0.174	0.971	0.417(7)	0.444(10)
(111)	0.213	−1.690	−0.367(8)	−0.413(15)
(002)	0.246	2.022	0.336(7)	0.376(13)
(112)	0.301	−1.363	0.336(11)	0.352(13)
(220)	0.348	−0.311	0.317(26)	0.318(26)
(003)	0.369	3.134	−0.254(7)	−0.304(15)
(221)	0.369	−2.941	−0.242(12)	−0.306(19)
(113)	0.408	−0.228	−0.242(20)	−0.242(20)
(222)	0.426	−2.616	0.253(10)	0.293(15)
(004)	0.492	3.385	0.192(8)	0.226(12)
(223)	0.507	−1.478	−0.229(7)	−0.238(7)
(330)	0.522	3.788	0.181(11)	0.235(16)
(114)	0.522	0.056	0.013(3)	0.013(3)
(331)	0.536	1.198	−0.217(9)	−0.223(9)
(332)	0.577	1.492	0.182(8)	0.190(9)
(224)	0.603	−1.187	0.176(9)	0.180(9)
(005)	0.615	0.794	−0.187(10)	−0.189(10)
(333)	0.639	2.590	−0.155(9)	−0.173(11)
(115)	0.639	−2.480	−0.143(6)	−0.155(7)
(440)	0.696	2.430	0.148(10)	0.162(11)
(441)	0.707	−0.094	−0.043(12)	−0.043(12)
(225)	0.707	−3.679	−0.093(12)	−0.110(13)
(334)	0.717	2.827	0.128(18)	0.143(19)
(006)	0.738	3.306	0.108(14)	0.123(14)
(442)	0.738	0.191	0.084(22)	0.085(22)
(116)	0.758	0.076	0.019(5)	0.019(5)
(443)	0.788	1.285	−0.128(63)	−0.131(63)
(335)	0.807	0.325	−0.112(20)	−0.112(20)
(226)	0.816	−1.130	0.094(9)	0.095(9)
(444)	0.852	1.520	0.099(12)	0.102(12)
(007)	0.861	2.945	−0.084(13)	−0.093(14)
(550)	0.870	−0.773	0.091(9)	0.092(9)
(551)	0.878	−3.213	−0.073(14)	−0.083(14)
(117)	0.878	−0.220	−0.053(11)	−0.053(11)
(552)	0.904	−2.933	0.064(13)	0.071(14)
(336)	0.904	2.764	0.075(18)	0.083(18)

the Ce form factor $f(\boldsymbol{Q})$ can be calculated by the tensor-operator method [18] with the radial integrals tabulated in [19].

The cerium wavefunctions can be determined in a simple model, by diagonalizing a Hamiltonian which contains the Heisenberg-like coupling in a mean field model and the crystal electric field (CEF) interaction,

$$H = H_Z + H_{ex} + H_{CEF}.$$

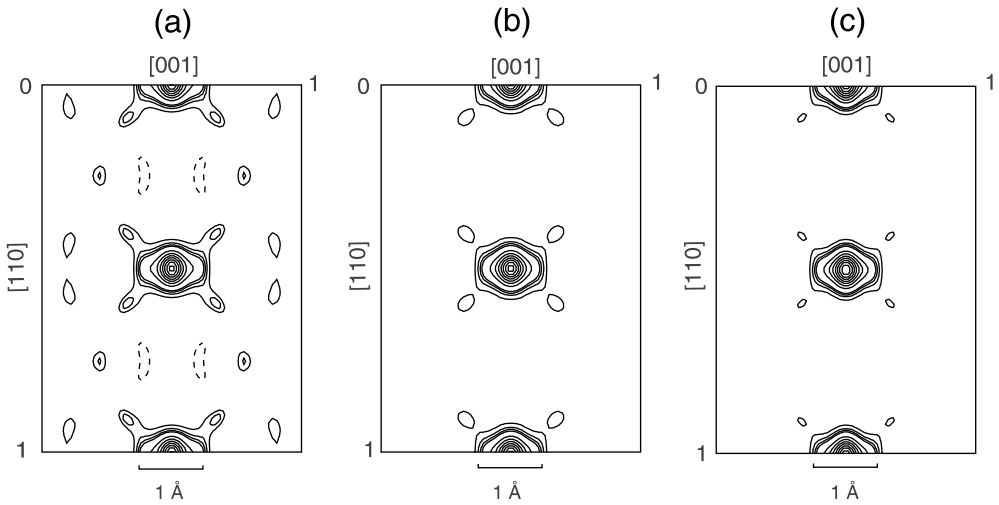

Figure 3. Magnetization distribution obtained with MaxEnt in CeB_6, in phase I (experiment 1). Projections along the $[1\bar{1}0]$ direction: (a) with all the measured reflections and no extinction corrections, (b) the same as (a) but without the very weak (114) reflection and (c) the same as (b) but with extinction corrections. The separation between the contour lines is 0.025 μ_B Å^{-2} for the negative and first four low contours. It is 0.150 μ_B Å^{-2} around the cerium sites.

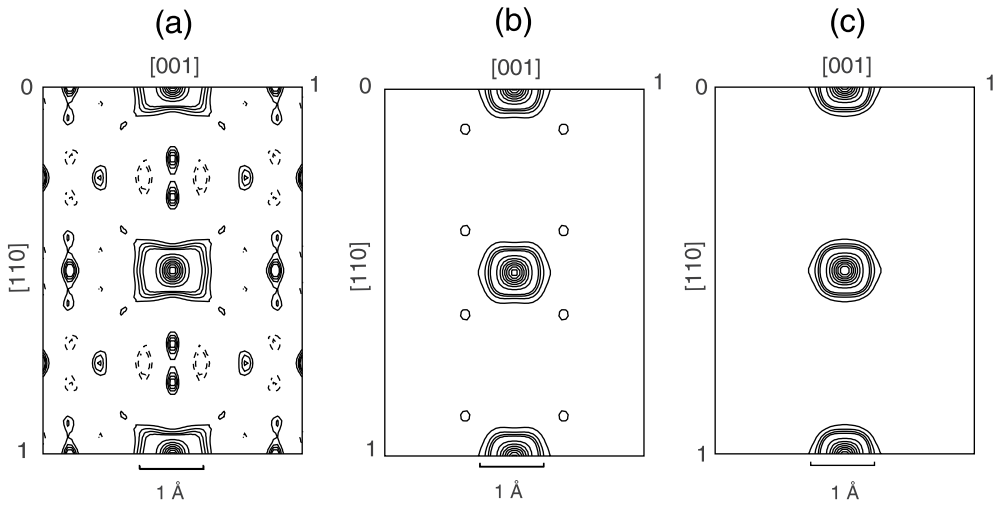

Figure 4. Magnetization distribution obtained with MaxEnt in CeB_6, in phase II (experiment 2). Projections along the $[1\bar{1}0]$ direction: (a) with all the measured reflections and no extinction corrections, (b) the same as (a) but without the very weak (114), (441) and (116) reflections and (c) the same as (b) but with extinction corrections. The separation between the contour lines is 0.05 μ_B Å^{-2} for the negative and first four low contours. It is 0.30 μ_B Å^{-2} around the cerium sites.

H_Z is the Zeeman contribution,

$$H_Z = -\boldsymbol{M} \cdot \boldsymbol{H}$$

and H_{ex} the exchange contribution, with an exchange coefficient n:

$$H_{ex} = -n\boldsymbol{M} \cdot \langle \boldsymbol{M} \rangle.$$

Table 5. Nuclear structure factors F_N and magnetic structure factors without extinction correction F_{M0} and with extinction correction F_M, for experiment 3 at ORNL with the field applied parallel to [001].

(hkl)	$\sin(\theta)/\lambda$ (Å^{-1})	F_N (10 fm/CeB$_6$)	F_{M0} $g = 0$ (μ_B/CeB$_6$)	F_M $g = 1000(300)$ (μ_B/CeB$_6$)
(000)	0.0		0.450(10)	
(100)	0.123	1.709	−0.365(10)	−0.450(25)
(110)	0.174	0.971	0.387(5)	0.402(7)
(200)	0.246	2.022	0.323(11)	0.379(18)
(210)	0.275	−0.630	−0.344(5)	−0.348(5)
(220)	0.348	−0.311	0.271(22)	0.271(22)
(300)	0.369	3.134	−0.214(11)	−0.278(19)
(310)	0.389	2.396	0.227(9)	0.256(12)
(320)	0.444	0.814	−0.222(12)	− 0.225(12)
(400)	0.492	3.385	0.209(19)	0.270(23)
(330)	0.522	3.788	0.136(12)	0.166(15)
(420)	0.550	1.085	0.169(8)	0.172(8)
(430)	0.615	2.188	−0.144(9)	−0.154(10)
(500)	0.615	0.794	−0.162(15)	−0.164(15)
(520)	0.662	−1.456	−0.113(9)	−0.116(10)
(440)	0.696	2.430	0.105(18)	0.114(18)
(530)	0.717	1.453	0.129(9)	0.133(9)
(600)	0.738	3.306	0.092(23)	0.119(24)
(610)	0.748	0.799	−0.119(21)	−0.120(21)
(620)	0.778	1.075	0.071(9)	0.073(9)
(630)	0.825	2.158	−0.095(13)	−0.102(13)
(700)	0.861	2.945	−0.087(14)	−0.110(16)
(550)	0.870	−0.773	0.076(20)	0.076(20)
(710)	0.870	2.224	0.085(12)	0.096(12)
(640)	0.887	2.380	0.083(21)	0.090(21)

The CEF contribution H_{CEF} is written

$$H_{CEF} = \sum_{l,m} B_{l,m} O_{l,m}.$$

For cubic symmetry the second order terms are zero, and in cerium the sixth order terms are also zero. The crystal elecric field contribution only depends on the fourth order crystal field term B_4. The $O_{l,m}$ are the Stevens operators, and for the field applied along a fourfold axis the CEF term is written [20]

$$H_{CEF} = B_4[O_4^0 + 5O_4^4]$$

whereas for the field applied along a twofold axis it is written

$$H_{CEF} = (-1/4)B_4[O_4^0 - 20O_4^2 - 15O_4^4].$$

In the presence of the CEF of cubic symmetry, the Ce^{3+} ion ground multiplet $J = 5/2$ is split into a Γ_7 doublet and a Γ_8 quartet. As evidenced by the previous form factor studies of Burlet *et al* [11], and then confirmed by several other studies [12–14], the fundamental level is the Γ_8 quartet. This configuration is related only to the sign of B_4 and is obtained for $B_4 < 0$.

Refinements of the experimental values of $\mu f(\boldsymbol{Q})$ were undertaken for the two experiments with the field applied along the twofold axis, in order to check the fundamental level and to get values of the crystal field and exchange parameters (B_4 and n, respectively). Three pairs

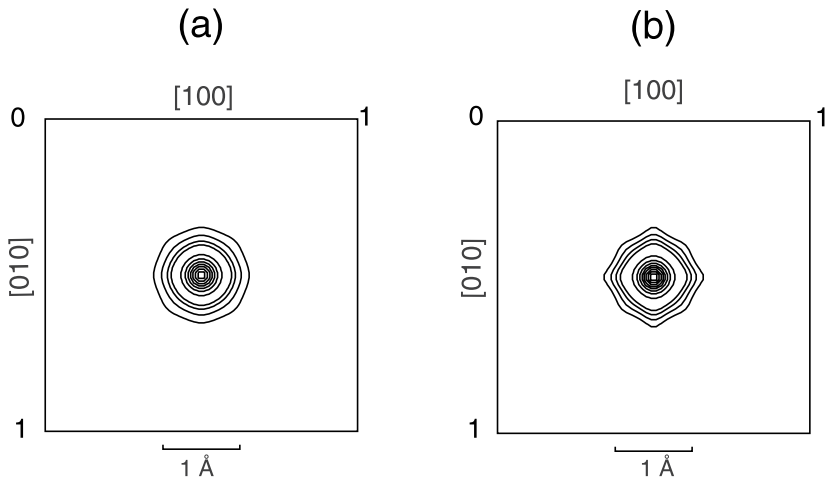

Figure 5. Magnetization distribution obtained with MaxEnt in CeB_6, in phase II (experiment 3). Projections along the [001] direction: (a) without extinction corrections and (b) with extinction corrections. The separation between the contour lines is 0.05 μ_B Å^{-2} for the first four low contours. It is 0.30 μ_B Å^{-2} around the cerium sites.

Table 6. Results of the form factor refinement (using $B_4 = -220$ K) for the two experiments with the field applied along the twofold axis. The values of χ^2 ($\chi^2 = \sum_i p_i (I_i^{obs} - I_i^{calc})^2/(N_{obs} - N_{var})$ with $p_i = 1/\sigma_i^2$) on all the reflections are 1.9 and 1.5 for experiments 1 and 2, respectively. If $B_4 > 0$, these values are 37 and 45, respectively. For three pairs of reflections, the μf calculated for $B_4 < 0$ (Γ_8 ground state) and $B_4 > 0$ (Γ_7 ground state) are compared.

Exp. no	T (K)	Exchange (K)	μ (μ_B)	$\sin\theta/\lambda$ (Å^{-1})	(hkl)	μf_{obs} (μ_B)	μf_{calc} for $B_4 < 0$ (μ_B)	μf_{calc} for $B_4 > 0$ (μ_B)
1	10	−5.2(0.1)	0.25	0.369	(221)	0.1642(97)	0.1676	0.1022
				0.369	(003)	0.1418(86)	0.1510	0.1575
				0.639	(333)	0.0941(95)	0.0830	0.0507
				0.639	(115)	0.0722(46)	0.0725	0.0969
				0.904	(552)	0.0372(75)	0.0401	−0.0082
				0.904	(336)	0.0218(69)	0.0343	0.0477
2	4.2	−1.8(0.1)	0.50	0.369	(221)	0.3064(199)	0.3389	0.2007
				0.369	(003)	0.3044(157)	0.3044	0.3182
				0.639	(333)	0.1729(110)	0.1678	0.1000
				0.639	(115)	0.1554(72)	0.1460	0.1986
				0.904	(552)	0.0707(142)	0.0813	−0.0213
				0.904	(336)	0.0831(185)	0.0693	0.0987

of reflections ((221) and (003), (333) and (115), and (552) and (336)) are at the same $\sin\theta/\lambda$. The μf values measured for the two reflections of each pair are different and the calculated ones depend on the sign of B_4. This experimental anisotropy in the μf is well described using $B_4 < 0$ (see table 6). Good reliability factors are obtained for a large set of negative B_4 values. $B_4 = -220$ K was chosen because it leads to a separation $\Delta = 500$ K between the Γ_8 quartet ground state and the Γ_7 doublet, as proposed in the literature [4, 13]. Then only the exchange parameter n was refined.

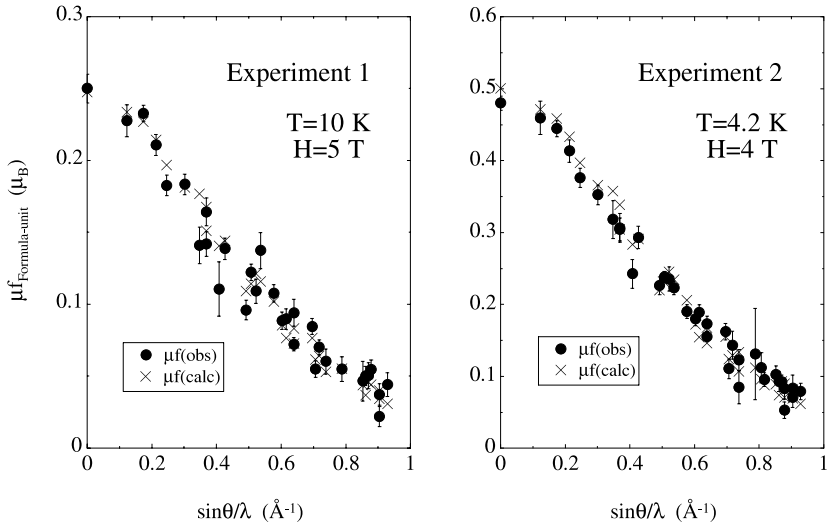

Figure 6. Comparison of observed and refined (using $B_4 = -220$ K) magnetic amplitudes $\mu f(\boldsymbol{Q})$ for the two experiments with the field applied along the twofold axis.

If a diffuse extra magnetization due to a polarization of conduction electrons were present, it would affect the low $\sin\theta/\lambda$ reflections [9] and disppear above $\sin\theta/\lambda \approx 0.3$ Å^{-1}. The first six reflections were not included in the refinement and the remaining reflections represent only the 4f contribution. Results of the refinement are gathered in table 6, and figure 6 shows the comparison between all observed and calculated $\mu f(\boldsymbol{Q})$. The agreement with a 4f calculation is quite good, even at low $\sin\theta/\lambda$, and one can confirm that no diffuse magnetization is observed. The refined values of the exchange coefficient n at the two temperatures are different. The less negative value at low temperature might be due to the fact that the Kondo state is destroyed rapidly with decreasing temperature [21].

Values of $\mu f(\boldsymbol{Q})$ for the field applied along a twofold or a fourfold axis, with the same crystal field and exchange parameters, have also been calculated. One can check in figure 7 that they are different ((hhl) and $(hk0)$ reflections, respectively). The difference is small for reflections of type $(00l)$, but quite important for reflections of type $(hh0)$, ranging from 2.3% for the (110) to 64% for the (550).

5. Conclusion

Programs based on the MaxEnt method have been used on previous and new polarized neutron measurements in two different phases of the compound CeB_6.

Although this new technique to obtain magnetization density maps is much more efficient than the classical Fourier synthesis, it is still important to perform the experiments as well as possible. For instance, short wavelengths minimize the extinction effects and allow collection of more data up to large values of $\sin\theta/\lambda$. The results of the measurements have also to be analysed with great caution and a critical mind. Data measured with the field applied along different axes of the cubic symmetry are not necessarily equivalent and cannot be mixed up. For peculiar reflections with very weak F_N values, the F_M, which is deduced from the flipping ratio R through $F_M = \gamma \times F_N$, is not well determined and it is better to use MaxEnt without these reflections than with wrong values.

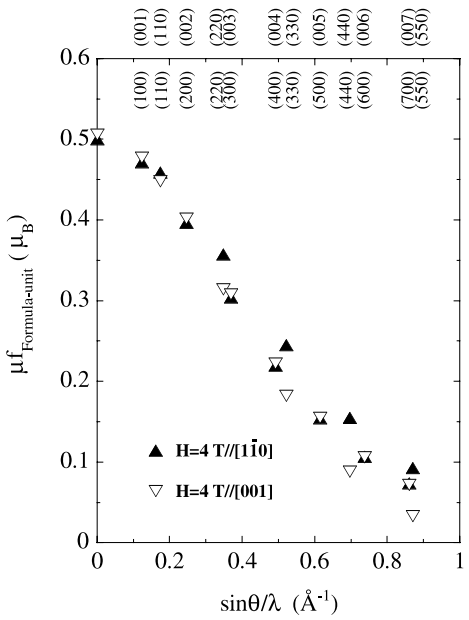

Figure 7. Values of $\mu f(\boldsymbol{Q})$ for the field applied along a twofold or a fourfold axis, with the same crystal field and exchange parameters ((*hhl*) and (*hk*0) reflections, respectively).

From our analysis, the 'anomalous spin density distribution' found by Saitoh *et al* [15] is essentially due to suspicious values for some reflections that are not suitable for flipping ratio measurements. We find that the magnetic density lies on the cerium sites only. Results are similar in both phases, I and II. The cerium form factor analysis also shows no extra delocalized contribution and confirms the 4f character of the CeB_6 magnetization. The Γ_8 quartet ground state of the Ce^{3+} in this Kondo compound is confirmed. However, no new information about the 'antiferro-quadrupolar' ordering can be obtained from these measurements, because we only deal with the magnetization component induced by the applied magnetic field.

References

[1] Fujita T, Suzuki M, Komatsubara T, Kunii S, Kasuya T and Ohtsuka T 1980 *Solid State Commun.* **35** 569
[2] Takase A, Kojima K, Komatsubara T and Kasuya T 1980 *Solid State Commun.* **36** 461
[3] Effantin J-M, Burlet P, Rossat-Mignot J, Kunii S and Kasuya T 1982 *Proc. Int. Conf. on Valence Instabilities (Zürich, 1982)* ed P Watcher (Amsterdam: North-Holland) p 559
[4] Effantin J-M, Rossat-Mignot J, Burlet P, Bartholin H, Kunii S and Kasuya T 1985 *J. Magn. Magn. Mater.* **47/48** 145
[5] Erkelens W A C, Regnault L-P, Burlet P, Rossat-Mignot J, Kunii S and Kasuya T 1987 *J. Magn. Magn. Mater.* **63/64** 61
[6] Takigawa M, Yasuoka H, Tanaka T and Ishizawa Y 1983 *J. Phys. Soc. Japan* **52** 728
[7] Hanzawa K 2000 *J. Phys. Soc. Japan* **69** 510
[8] Shiina R 2002 *J. Phys. Soc. Japan* **71** 2257
[9] Alonso J A, Boucherle J-X, Givord F, Schweizer J, Gillon B and Lejay P 1998 *J. Magn. Magn. Mater.* **177–181** 1048
[10] Boucherle J-X and Schweizer J 1985 *Physica* B **130** 337
[11] Burlet P, Boucherle J-X, Rossat-Mignot J, Cable J W, Koehler W C, Kunii S and Kasuya T 1982 *J. Physique* **43** C7–273
[12] Loewenhaupt M and Carpenter J M 1983 *IPNS Prog. Rep., Argonne* p 132

[13] Sato N, Kunii S, Oguro I, Komatsubara T and Kasuya T 1984 *J. Phys. Soc. Japan* **53** 3967
[14] Peysson Y, Ayache C, Salce B, Rossat-Mignot J, Kunii S and Kasuya T 1985 *J. Magn. Magn. Mater.* **47/48** 63
[15] Saitoh M, Okada N, Nishibori E, Takagiwa H, Yokoo T, Nishi M, Kakurai K, Kunii S, Takata M, Sakata M and Akimitsu J 2002 *J. Phys. Soc. Japan* **71** 2369
[16] Schenck A, Gygax F N and Kunii S 2002 *Phys. Rev. Lett.* **89** 037201
[17] Papoular R J and Gillon B 1990 *Europhys. Lett.* **13** 429
[18] Lovesey S W and Rimmer D E 1969 *Rep. Prog. Phys.* **32** 333
[19] Freeman A J and Desclaux J-P 1979 *J. Magn. Magn. Mater.* **12** 11
[20] Hutchings M T 1964 *Solid State Phys.* **16** 227
[21] Kawakami M, Kunii S, Komatsubara T and Kasuya T 1980 *Solid State Commun.* **36** 435